Nanomedicine: Nanotechnology, Biology, and Medicine 62 (2024) 102784

Contents lists available at ScienceDirect

Nanomedicine: Nanotechnology, Biology, and Medicine

journal homepage: www.sciencedirect.com/journal/nanomedicine-nanotechnology-biology-and-medicine

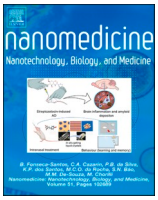

A novel mertansine conjugate for acid-reversible targeted drug delivery validated through the Avidin-Nucleic-Acid-NanoASsembly platform

Elisa Schiavon, MSc [a,1], Sara Rezzola, PhD [b,1], Erica Filippi, MSc [a], Marta Turati, PhD [b], Sofia Parrasia, PhD [c], Simone Bernardotto, MSc [a], Martina Stocco, MSc [a], Ildikò Szabò, PhD [c], Andrea Mattarei, PhD [a], Roberto Ronca, PhD [b,2,*], Margherita Morpurgo, PhD [a,*,2]

[a] Pharmaceutical and Pharmacological Sciences Dept (DSF), University of Padova, Via Marzolo, 5. 35131 Padova, Italy
[b] Molecular and Translational Medicine Dept (DMMT), University of Brescia, v.le Europa 11, 25121 Brescia, Italy
[c] Department of Biology (DiBio), University of Padova, Via U. Bassi, 58/B, Padova, Italy

ARTICLE INFO

Keywords:
Targeted therapeutics
cancer
Reversible conjugates
Mertansine
DM1
Avidin-biotin
Avidin-Nucleic-Acid-NanoASsembly

ABSTRACT

In targeted cancer therapy, antibody-drug-conjugates using mertansine (DM1)-based cytotoxic compounds rely on covalent bonds for drug conjugation. Consequently, the cytotoxic DM1 derivative released upon their proteolytic digestion is up to 1000-fold less potent than DM1 and lacks a bystander effect. To overcome these limitations, we developed a DM1 derivative (keto-DM1) suitable for bioconjugation through an acid-reversible hydrazone bond. Its acid-reversible hydrazone conjugate with biotin (B-Hz-DM1) was generated and tested for efficacy using the cetuximab-targeted Avidin-Nucleic-Acid-NanoASsembly (ANANAS) nanoparticle (NP) platform.

NP-tethered B-Hz-DM1 is stable at neutral pH and releases its active moiety only in endosome/lysosome mimicking acidic pH. *In vitro*, the NP/Cetux/B-Hz-DM1 assembly showed high potency on MDA-MB231 breast cancer cells. *In vivo* both B-Hz-DM1 and NP/Cetux/B-Hz-DM1 reduced tumor growth. A significantly major effect was exerted by the nanoformulation, associated with an increased *in situ* tumor cell death. Keto-DM1 is a promising acid-reversible mertansine derivative for targeted delivery in cancer therapy.

Background

As of today, the early dream of selective drug delivery only at the body site where it is needed is being pursued through the development of various drug delivery systems with different geometries. In the field of cancer therapy, the first representatives approved for clinical practice have been the antibody drug conjugates (ADCs), *i.e.* monoclonal antibodies (mAbs) linked to cytotoxic drugs that can recognize cancer-specific epitopes. ADCs are currently among the fastest-growing drug classes in oncology.[1,2] The same working principle as ADCs may be also pursued by alternative geometries, including targeted nanoparticles (NPs), *e.g.*, liposomes, micelles, and others.[3] Despite their greater formulation complexity, which in part is responsible for their slower clinical translation, some of these macromolecular systems have shown high potential and, in some situations, superior properties when compared to the corresponding ADCs.[4,5]

Several decades of research in this field have led to the identification of key elements affecting the efficacy of ADCs, some of which are also shared by other targeted delivery systems. These include: i) the proper selection of cancer-specific antigens for mAb targeting; ii) the nature of the cytotoxic moiety and its ability (or inability) to exert a bystander effect, namely the possibility of affecting neighboring cells not directly reached by the antibody-driven drug; iii) the chemistry of the linker for drug tethering.

The cytotoxic ADC moieties currently used in clinical practice belong to four main classes of compounds and include the mayntansinoids,[1] which are microtubulin polymerization inhibitors derived from natural maytansine. Maytansine has an *in vitro* IC_{50} potency in the pM range,

Abbreviations: ANANAS, Avidin-Nucleic-Acid-NanoASsembly; DM1, mertansine; Cetux, cetuximab.

* Corresponding authors.
E-mail addresses: roberto.ronca@unibs.it (R. Ronca), margherita.morpurgo@unipd.it (M. Morpurgo).

[1] ES and SR contributed equally to the manuscript.
[2] MM and RR share the last/senior authorship.

https://doi.org/10.1016/j.nano.2024.102784
Received in revised form 27 June 2024;
Available online 3 September 2024

below the typical concentration reached by therapeutic antibodies at the tumor site, making it suitable for ADC development. Over the years, three semisynthetic derivatives (*i.e.* DM1-Mertansine, DM3 and DM4) incorporating a thiol function into the Maytansine C3 ester side chain[6,7] were developed to permit conjugation of maytansinoid compounds to mAbs.[8,9] These derivatives have become the building blocks for the preparation of current maytansinoid-based conjugates, in which the active element can be linked through different chemistries. In Kadcyla (trastuzumab emtansine T-DM1, the only clinically approved maytansinoid conjugate), DM1 is linked to the mAb using a covalent approach so that the released active element is a lysine conjugate (DM1-Lys). This derivative has been shown to be up to 1000 times less cytotoxic than DM1[10] and, due to its hydrophilic nature, is unable to cross cell membranes, thus lacking the bystander effect.[11]

A strategy to overcome these drawbacks is the use of reversible disulfide-based (SS) linkers, which are designed to release the more potent DM1.[12–14] However, no product with this chemistry has been clinically approved so far. Actually, SS-based mertansine conjugates have often demonstrated poor potency *in vivo*,[11,15] probably because drug release from the SS-based bioconjugates depends on their ability to reach the cytoplasm of target cells,[10] and this depends on their cell trafficking properties.[1,7,11]

Another option for reversible drug tethering, often adopted in ADCs, is represented by acid-sensitive reversible bonds. This approach is ideal in the case of delivery systems that enter target cells *via* the endosome/acid lysosome route as, for example, NP-based systems. However, to date, no maytansine derivative suitable for this chemistry has been developed.

Along with the development of novel linkers for targeted drug conjugates (such as ADCs), several variables independent of the linker chemistry itself influence the efficacy of a targeted delivery system. These include the site of drug tethering onto the targeting agent and the ratio between the active molecule and the targeting agent (DAR; Drug-to-Antibody Ratio in ADCs). In practical terms, it is not simple to control these variables in such a way that the results correlate *only* with the chemistry under investigation.

A potential tool to bypass this risk of biased results is represented by the Avidin-Nucleic-Acid-Nano-ASsemblies (ANANAS) platform. ANANAS are a class of soft and fully biocompatible poly-avidin nanoparticles[16] that form upon the high affinity driven nucleation of avidin units around a noncoding plasmid DNA.[16,17] Thanks to this high affinity interaction, these NPs possess a highly defined and reproducible composition with about 350 avidins/NP.[17,18] The large number of biotin binding sites (BBS) of ANANAS are available for docking with stoichiometric control (thanks to the high affinity of the avidin-biotin interaction, Kd = 10^{-15} M), different functional elements (drugs, fluorophores for tracking and/or targeting elements), provided these are linked to a biotin moiety.

Application of this platform has been described in the context of *in vitro* and *in vivo* diagnostics[17,19–21] and in drug delivery.[4,22] In addition, thanks to the possibility to finely tune the composition of multifunctional ANANAS, the platform has been used as a tool to probe surface composition/function relationships in nanotechnology.[23,24] Notably, ANANAS enter cells *via* the endosome/lysosome pathway.[4,25] Therefore, by generating biotin-linked drug conjugates with different linker chemistries, this platform can be used as a tool to compare the linker chemistries meant to be used within drug delivery systems that follow this path of cell internalization[23] (Fig. S1).

In this work, we designed and investigated the potential of a novel DM1 derivative carrying a keto function (Keto-DM1) suitable for bioconjugation through an acid-reversible hydrazone bond. To investigate its possible application for mAb-targeted therapies, we generated the acid-reversible conjugate with biotin (*i.e.* B-Hz-DM1). Moreover, to test its anti-tumor potential, B-Hz-DM1 was formulated within an Epidermal Growth Factor Receptor (EGFR)-targeted ANANAS (using the anti-EGFR mAb Cetuximab) and evaluated *in vitro* and *in vivo*. Our results reveal a significant therapeutic profile of this new DM1 derivative compared to that exerted by the covalent conjugate (*i.e.* B-MPA-DM1).

Methods

Materials and instrumentation

Biotin, N,N-Diisopropylethylamine (DIPEA), triethylamine (TEA), trifluoroacetic acid (TFA), N-Boc-1,6-diaminohexane, N,N′-dicyclohexylcarbodiimide (DCC), N-hydroxysuccinimide (NHS), N,N′-dicyclohexylcarbodiimide, 3-(Maleimido)propionic phtalimide, 6-chlorohexan-2-one were purchased from Sigma-Aldrich. α-biotin, ω succinimidyl valerate poly(ethylene glycol), MW 5000 (biotin-PEG5kDa-SVA), α-biotin, ω methoxy, poly(ethylene glycol), MW 5000 (biotin-PEG5kDa-methoxy, biotin-mPEG) were purchased from Laysan Bio (Huntsville, AL, USA). Solvents were purchased from Merck Sigma-Aldrich or Carlo Erba, Cornaredo-MI, IT). Biotin-C6-Lys(methoxyPEG5kDa)$_2$ was synthesized as described elsewhere[17]; Mertansine (DM1) was purchased from D.B.A. Italia S.r.l. (Segrate, MI, Italy); Avidin was purchased from e.protein (Belgium). Cetuximab (Erbitux®, lot G015SR) was purchased from Merck Serono. NMR experiments were performed on a Bruker Avance III 400 spectrometer (frequencies: 400.13 and 100.62 MHz for ^{1}H, and ^{13}C nuclei, respectively) equipped with a multinuclear inverse z-field gradient probe head (5 mm). For data processing, TopSpin 4.0.8 software was used and the spectra were calibrated using solvent signal ($CDCl_3$ ^{1}H 7.26 ppm ^{13}C 77.16, DMSO ^{1}H 2.50 ppm ^{13}C 39.52, D_2O 1H 4.79 ppm). Multiplicities are reported as follows: s, singlet; d, doublet; t, triplet; q, quartet; m, multiplet; b, broad; dd, doublet of doublets. Reverse-phase high-performance liquid chromatography (RP-HPLC) analyses were carried out with an Agilent chromatography system (USA), model 1220 Infinity LC equipped with diode array detector, using a Phenomenex Kinetex C18 5 μm 4.6 mm × 250 mm) column. Mass spectra were recorded by direct infusion ESI on a Thermo Fisher Scientific LCQ Fleet ion trap mass spectrometer. Dynamic light scattering measurements were performed with a Malvern Zetsizer nano- ZS, UV–Vis spectra were recorded with a Varian Cary 50 UV–Vis spectrophotometer.

Synthesis

Biotin-PEG$_{5kDa}$-Cetuximab was obtained by mixing Cetuximab (1 mg/mL in 10 mM phosphate, 150 mM NaCl, pH 7.4-PBS) and biotin-PEG-SVA at PEG:Cetuximab 10:1 M ratio. The product was purified by ultrafiltration (Amicon® appartus, cut off 30 kDa). The average number of biotin-PEG/antibody was measured by the iodine assay[26] and confirmed by biotin titration.[27] The ability of the conjugate to tether the ANANAS particles was verified by mixing the product with core ANANAS in PBS at IgG/NP molar ratio = 30:1 and analyzing the mixture by gel permeation chromatography (Akta purifier®, Cytiva) in a Superose 6 prep® medium (Tricorn®10/300) (Fig. S4)

Biotin-DM1 conjugates B-MPA-DM1 (4), B-Hz-DM1 (12) and keto-DM1 (13) were obtained by classic organic synthesis procedures as detailed in the supplementary information (S.I.) file. Compound identity was verified by ^{1}NMR and Mass Spectroscopy. Purity was assessed by RP-HPLC.

Functional nanoparticle assembly

Non-functionalized ANANAS "core" assemblies were obtained in freeze-dried form according to optimized procedures published elsewhere.[17] Core NPs were reconstituted at 1 mg/mL in 10 mM phosphate, 150 mM NaCl, Tween20 0.012 % p/v, pH 7.4 (PBS-T) buffer and added of the biotinylated elements to the desired biotin/BBS molar ratio. Assembly size was determined by dynamic light scattering (DLS) using a Malvern Ultrasizer apparatus in the presence of 0.1 % w/v fetal calf serum (FCS).

Stability of B-Hz-DM1 to hydrolysis

The stability of compound B-Hz-DM1 both as a free molecule and when linked to the NPs (biotin:available BBS = 1:2) was examined in different aqueous media (5 mM phosphate pH 7.4, 100 mM phosphate pH 7.4:DMSO 80:20; 10 mM Na citrate, pH 5.5). Solutions (10^{-5} M in DM1) were incubated in the selected buffer at 37 °C, and at scheduled time points they were analyzed by reverse-phase high-performance liquid chromatography (RP-HPLC). Before HPLC analysis, the protein fraction was removed from the solution by cold acetone precipitation. RP-HPLC analyses were carried out with an Agilent chromatography system (USA), model 1220 Infinity LC equipped with diode array detector, using a Phenomenex Kinetex C18 5 μm 4.6 mm × 250 mm) column (Eluent A, buffer triethylammonium bicarbonate pH 7.4; eluent B, ACN; gradient from 10 % to 90 % B in 40 min).

Cell cultures

Human MDA-MB-231, SKBR3 and U87MG cell lines were obtained from ATCC. MDA-MB-231 and U87MG cells were cultured in DMEM *plus* 10 % FBS, whereas SKBR3 cells were maintained in McCoy's 5A medium *plus* 20 % FBS. Cells were kept at low passage, used at passages between 25 and 30, and regularly tested for lack of Mycoplasma.

Cell proliferation assay

MDA-MB-231, SKBR3 or U87MG cancer cells were seeded in 48-well plates at 12,500 cells/cm^2. After 24 h, cells were treated in the appropriate medium *plus* 1 % FBS with increasing concentrations (0.001 nM–10 μM) of DM1, B-MPA-DM1, B-Hz-DM1, or Keto-DM1. After 72 h of incubation, cells were trypsinized. Absolute cell count was obtained by the counting function of the MACSQuant Analyzer (Miltenyi Biotec).

As for the cytotoxicity of ANANAS tethered biotin conjugates, MDA-MB-231 cells were seeded in 48-well plates at 12,500 cells/cm^2 and treated for 72 h with increasing concentrations of B-Hz-DM1, NP/B-Hz-DM1, NP/Cetux/B-Hz-DM1 or B-MPA-DM1, NP/B-MPA-DM1, NP/Cetux/B-MPA-DM1 (DM1 derivatives ranging from 0.1 nM to 100 nM). Then, cells were counted as reported above.

In vivo antitumor assay

Animal experiments were approved by the local animal ethics committee (Organismo Preposto al Benessere degli Animali (OPBA), University of Brescia, Italy) and were performed in accordance with national guidelines and regulations. Seven-week-old female NOD/SCID mice were injected orthotopically with 3×10^6 human MDA-MB231 cells in 20 μL total volume of PBS into the mammary fat pad. When tumors were palpable (~80 mm^3), mice were randomized (n = 6–8 mice/group) and treated or not twice a week by i.v. injection with 100 μL of B-Hz-DM1 (46.6 μg/dose, equivalent to 27.7 μg or 1.11 mg/Kg in DM1), NP/Cetux (1 mg/dose, equivalent to 40 mg/Kg in nanoparticles), NP/Cetux/B-Hz-DM1 (27.7 μg equiv or 1.11 mg/Kg in DM1 and 1 mg/dose–40 mg/kg in Nanoparticles and 70 μg IgG or 2.8 mg/kg in Cetuximab). Tumors were measured in two dimensions and tumor volume was calculated according to the formula V 1/4 ($D \times d^2$)/2, where D and d are the major and minor perpendicular tumor diameters, respectively. At the end of the experimental procedure, tumors were harvested, weighted, and analyzed by immunohistochemistry.

Immunohistochemical analysis

7 μm-thick tumor sections were deparaffinized and rehydrated. Antigen retrieval was performed warming the sections into pre-warmed citrate buffer (10 mM, pH 6) in a microwave oven (160 W for 15 min). The sections were then stained using the Mouse to Mouse HRP kit (ScyTek Laboratories), according to the manufacturer's instructions. Ki67 was stained using anti-rabbit Ki67 primary antibody (Abcam ab16667). The sections were counterstained with hematoxylin and dehydrated. 8 fields were randomly captured from each section and analyzed as follows. Each picture was deconvolved in DAB and hematoxylin staining and nuclei were counted in order to calculate Ki67 index as the percentage of DAB positive nuclei and total nuclei. For TUNEL assay, the TUNEL Assay Kit - HRP-DAB (ab206386) was used. Counterstaining was performed using Methyl Green provided by the kit and dehydrated. Each section was captured with a Leica DM6 microscope (10× lens). DAB positive apoptotic areas were measured with ImageJ software and expressed as percentage of the total slice area.

Results

Synthesis and characterization of biotin-DM1 conjugates

Two biotin DM1 derivatives to be loaded on the ANANAS polyavidin carrier (B-MPA-DM1 and B-Hz-DM1, Fig. 1) were designed with either acid-sensitive or covalent linker strategies (synthesis details in Supporting Information). In both derivatives, the DM1 thiol function was exploited to introduce a N-butyl-3-(2,5-dioxopyrrolidin-1-yl) propanamide spacer, which was further functionalized.

For the acid-reversible approach, we inserted a hydrazone, namely a pH sensitive bond deriving from the condensation of a hydrazine with a keto (or aldehyde) function. To favor crossing of cell membrane by the active moiety, we introduced the more hydrophobic *keto* function within the DM1 portion of the conjugate (Keto-DM1, Fig. 1) and the more hydrophilic hydrazine function within the biotin carrier element. In this way, the resulting acid-released keto-DM1 is more hydrophobic than DM1-Lys. For the covalent approach, we used an amide bond between the spacer and biotin. In this case, the B-MPA-DM1 conjugate is expected to be released from the carrier upon proteolytic digestion of the NPs, similar to what occurs in Kadcyla. In both hydrazone and covalent conjugates, the distance between biotin and DM1 was longer than the minimum 6 carbons necessary for optimal avidin tethering.[28]

In order to assess the pH dependent sensitivity of B-Hz-DM, its hydrolytic stability at 37 °C was evaluated in different pH environments for up to 24 h, by combining HPLC and mass spectrometry (see also Table S1). As shown in Fig. 2, hydrazone hydrolysis in B-Hz-DM1 displayed a strong pH dependence: at neutral pH, the release in solution of keto-DM1 from B-Hz-DM1 occurred with an average rate of 4.8 %/hour, whereas at acidic pH full hydrolysis occurred within 2 h (release >70 %/hour). Notably, ANANAS tethering of B-Hz-DM1 (BBS:biotin molar ratio equal to 2) provided a strong stabilization of the hydrazine. Indeed, when B-Hz-DM1 was linked to the NPs, no release of keto-DM1 was registered at neutral pH for at least 24 h, while at low pH the release rate was of about 6 %/hour, at least ten-fold slower than when tested as a free molecule.

In vitro cytotoxicity of free molecules

The cytotoxic potential of the biotinylated compounds was preliminarily evaluated *in vitro* on a panel of human tumor cell lines including breast cancer (MDA-MB-231 and SKBR3) and glioblastoma (U87MG) cells. MDA-MB-231 is a highly aggressive triple negative breast cancer cell line, while SKBR3 is a human breast cancer cell line that overexpresses the Her2 gene product (therefore it is a useful model for investigating resistance to Her2-targeted therapies) and harbors p53 R175H mutation. As shown in Fig. 3, and summarized in Table 1, the treatment with DM1 and its derivatives significantly impaired the growth of all three tumor cell lines, thus proving that the chemical modification and conjugation procedures did not affect the cytotoxic potential of the drugs.

As shown in Table 1, the biotinylated derivatives B-MPA-DM1 and B-Hz-DM1 have a comparable IC_{50} concentration range (105–190 nM), whereas the keto-DM1 derivative (representing the free/hydrolyzed

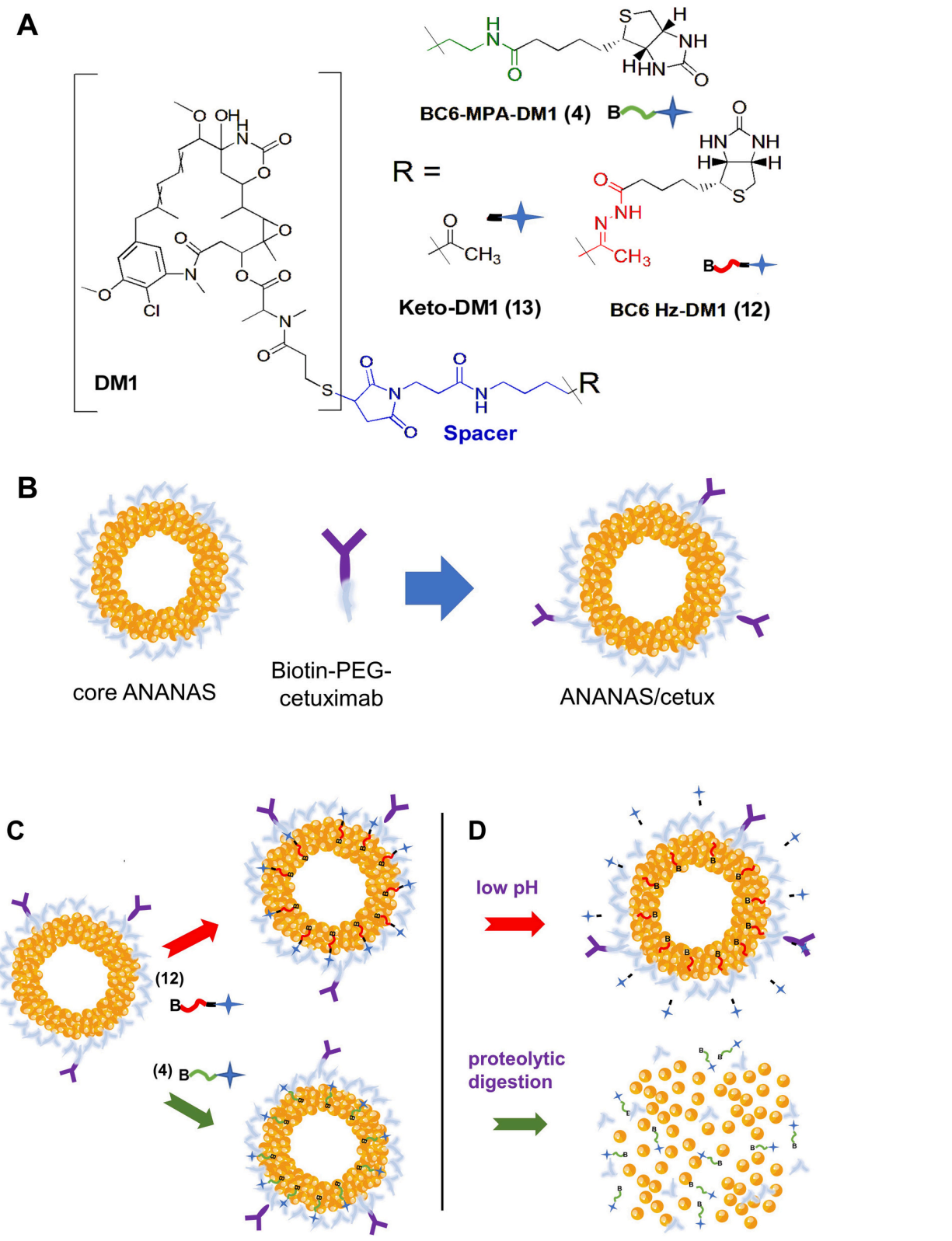

Fig. 1. Schematic representation of the DM1 conjugates, the nanoassembly procedure, and the working principle of the NP-tethered DM1. A) DM1 was tethered to biotin through a covalent linker (B-MPA-DM1 or compound 4, linker in green) or using an acid reversible hydrazone (B-Hz-DM1 or compound 12, linker in red). All compounds share an additional spacer (in blue) between DM1 and the linker. B) Scheme of functional assembly of ANANAS/Cetuximab complexes. C) Assembly of B-MPA-DM1 and B-Hz-DM1 onto ANANAS/Cetuximab complex occurs through the avidin-biotin interaction. D) Release of the cytotoxic moiety is triggered by either acid pH or proteolytic digestion of the assembly. Acid-driven hydrolysis of B-Hz-DM1 yields the keto derivative Keto-DM1, whereas the proteolytic digestion of NPs releases B-MPA-DM1.

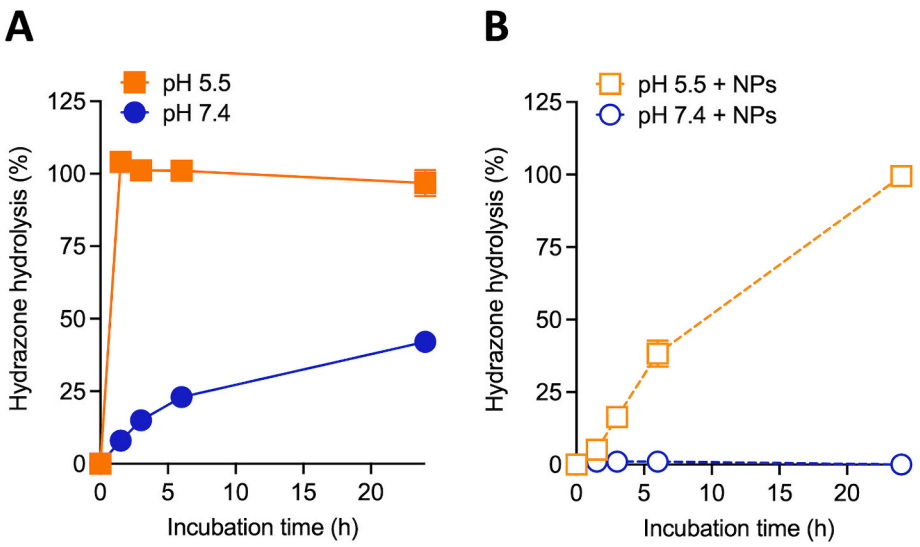

Fig. 2. Kinetics of hydrolysis of B-Hz-DM1 at pH 5.5 and pH 7.4. The release of Keto-DM1 was measured in the absence (A, full signs) or in the presence (B, empty signs) of NPs at neutral or acidic pH (circles or square symbols, respectively). Additional data related to hydrolysis are reported in Supplementary Information file.

derivative released from B-Hz-DM1) displays a slightly lower IC_{50}. Indeed, among all the compounds, keto-DM1 was the most active, with an IC_{50} between 65 and 100 nM depending on the cell line, and an overall 4-to-17-fold potency loss with respect to the parental DM1. This is of relevance considering that up to 1000-fold potency loss for the DM1-Lys conjugate is documented.[10,12]

ANANAS-based formulations

Given the promising efficacy of B-MPA-DM1 and B-Hz-DM1, the conjugates were tethered to ANANAS-based NPs. Core ANANAS possesses about 1000 biotin binding sites (BBS) available for docking biotinylated functional elements. In principle, as long as the number of available BBS or the surface available (~6000 nm^2) is not exceeded,[18] quantitative docking of the biotinylated elements at the NP surface should occur, allowing the assembly solutions to be used without the need of purification. Considering that each biotinylated moiety displays an individual molecular footprint (*e.g.* the surface area occupied by a single molecule), pre-formulation studies are always necessary to verify the maximal NP loading capability for the different biotin elements and the colloidal stability of final formulations.

To provide the specific targeting towards EGFR-expressing tumor cells, 10 molecules of Cetuximab-biotin were added to each NP (NP/Cetux). This amount of targeting antibody, which is much lower than the maximum ANANAS capacity for IgG (equal to 60 molecules/NP,[18] was demonstrated as the most effective to target NPs towards $EGFR^+$ tumor cells.[4] To estimate the maximal loading capacity of NP/Cetux for each of the two biotin-DM1 conjugates, the NP/IgG assembly was mixed with the desired biotinylated moiety at 60 % and 120 % theoretical BBS coverage and the solution mixtures were analyzed by gel permeation chromatography (Fig. 4A–C). The amount of biotin conjugates unretained by the NPs was estimated from the area of the peaks at 26.16 mL (B-Hz-DM1) or 26.88 mL (B-MPA-DM1) retention volume, corresponding to the conjugates when free in solution. The NP/cetux loading capability for both conjugates was found to correspond to 60 % BBS coverage, which matches to about 800 molecules/NP, close to the theoretical maximum capability based on available BBS and in line with the fact that the 10 Cetuximab moieties introduced for targeting occupy about 17 % of the available surface area. All DM1 loaded assemblies were colloidally stable, as demonstrated by Dynamic light scattering (Figs. 4D–F and S5). Depending on the composition, the assemblies displayed a size between 155 and 168 nm. Core NPs (about 155 nm) consist of the inner poly-avidin core surrounded by the outer surface layer generated by the 5 kDa biotin-PEG added as colloidal stabilizer. Addition of the large MW biotin-PEGylated (5 kDa) IgG leads to a size increase of about 10 nm, in agreement with its positioning at the external surface of the NP outer PEG layer. Addition of the smaller biotin-DM1 conjugates has minor effect on the NP size (size increase ~1.5–3 nm), consistent with their positioning in proximity with the protein NP core.

In vitro cytotoxicity of ANANAS tethered biotin conjugates

The cytotoxic potential of the biotin-conjugates tethered to the NPs was assessed *in vitro* on the human triple negative breast cancer MDA-MB-231 cells. These cells express EGFR, are efficiently recognized by the anti-EGFR antibody Cetuximab, and the capacity of Cetuximab-guided ANANAS to recognize and to be internalized in MDA-MB-231 cells has already been reported.[4]

As shown in Fig. 5A, at the doses tested (ranging from 0.1 to 100 nM) the covalent derivative B-MPA-DM1 alone had no significant cytotoxic effect on MDA-MB-231 cells. Notably, its efficacy was only slightly enhanced by conjugation and loading on the EGFR-targeted NPs (NP/Cetux/B-MPA-DM1). Indeed, these formulations displayed a dose-response pattern similar to the drug-free NPs carrying Cetuximab only (NP/Cetux). On the contrary, the cytotoxicity of the hydrazone derivative was dramatically enhanced upon loading onto EGFR-targeted ANANAS (Fig. 5B). These data are the result of the enhanced conveyance capacity of the mAb (Cetuximab) together with the superior cell internalization properties of the nanoformulation and the efficient acid-mediated release of the drug by the linker. Altogether, these data prove the enhanced activity of the new acid cleavable B-Hz-DM1 compound in its targeted-ANANAS loaded formulation (Fig. 5C), thus setting the basis for further *in vivo* validation.

In vivo efficacy of ANANAS tethered B-Hz-DM1 conjugate

The anti-tumor potential of the DM1 hydrazone derivative B-Hz-DM1 loaded on EGFR-targeted NPs was assessed *in vivo* in a human triple negative breast cancer model. To this aim, MDA-MB-231 cells were orthotopically injected into immune-deficient mice. Once tumors were palpable, mice were treated twice a week with the B-Hz-DM1 alone or conjugated with the Cetuximab-loaded NPs (NP/Cetux/B-Hz-DM1). The equivalent dose of DM1 per treatment was equal to 0.03 mg

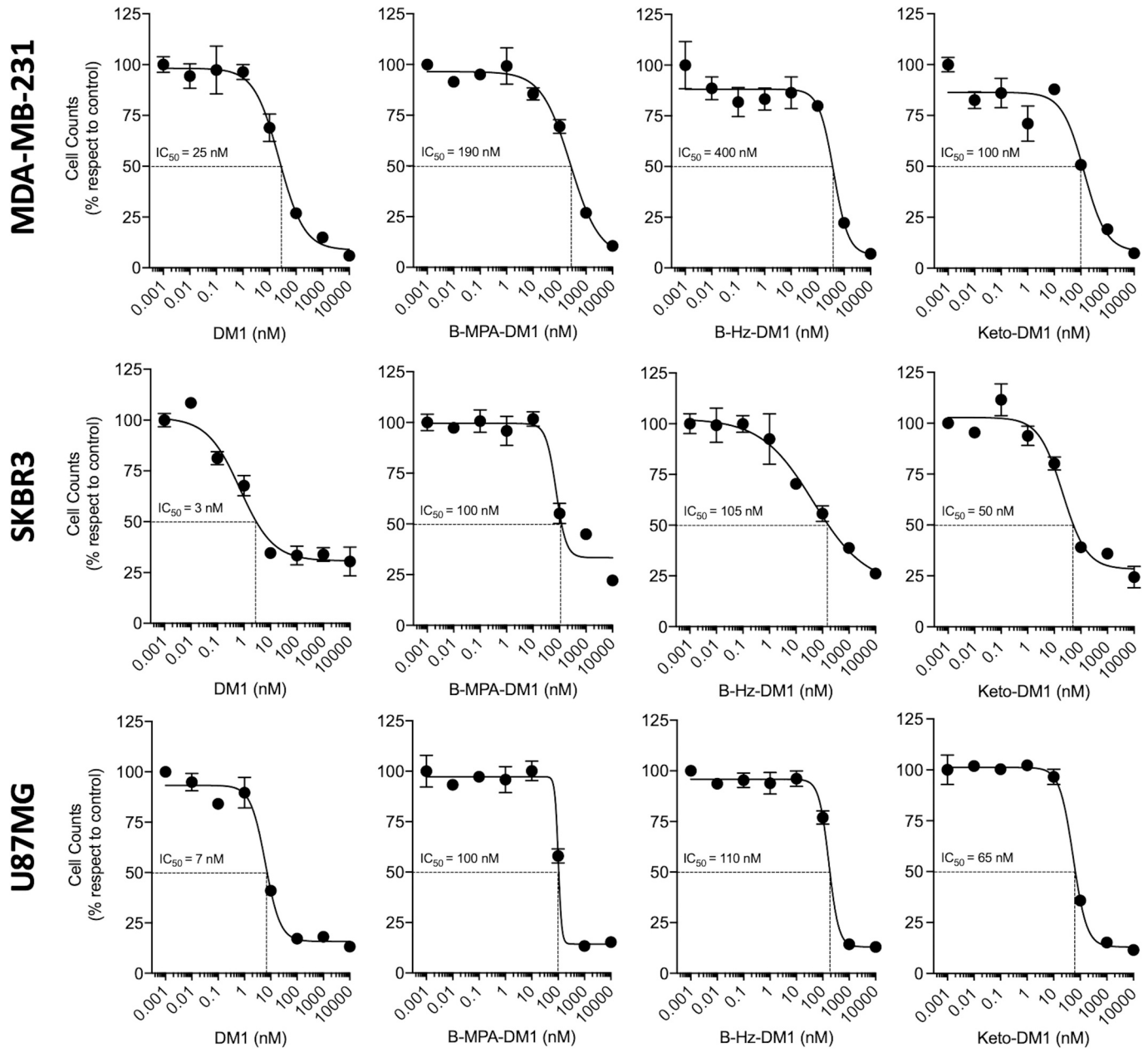

Fig. 3. Effect of DM1 ant its derivatives on tumor cells. Viable cell counts of MDA-MB-231, SKBR3 and U87MG tumor cells treated for 72 h with increasing concentration of the indicated compound. The graphs report the percentage of live cells in respect to the control and the estimated IC_{50} value for each treatment condition. Results are the mean ± SEM.

Table 1
Summary table of the IC_{50} values for DM1 and the new DM1-conjugates tested on the different human cancer cell lines.

	IC50 (nM)		
	MDA-MB-231	SKBR3	U87MG
DM1	25	3	7
B-MPA-DM1	190	100	100
B-Hz-DM1	110	105	110
Keto-DM1	100	50	65

(corresponding to 1.2 mg/Kg), in line with doses used to evaluate other DM1 conjugates.[29,30] Cetuximab-loaded NPs (NP/Cetux) and vehicle (control) were used as reference controls.

As shown in Fig. 6A–B, B-Hz-DM1 alone displayed a relevant anti-tumor effect significantly reducing both tumor volume and weight in comparison with control (297.0 ± 26.6 mm^3 *vs* 402.8 ± 19.0 mm^3). Notably, and in accordance with what observed *in vitro*, the EGFR-targeted NP-loaded NP/Cetux/B-Hz-DM1 formulation displayed stronger effect on tumor growth both when compared with control (209.2 ± 19.9 mm^3 *vs* 402.8 ± 19.0 mm^3) and when compared with the unloaded B-Hz-DM1 derivative (209.2 ± 19.9 mm^3 *vs* 297.0 ± 26.6 mm^3). Moreover, immunohistochemical analysis of tumor plugs revealed that both treatments significantly reduced cell proliferation inside the tumors, as assessed by the standardized biomarker Ki67 (Fig. 6C). Indeed, the percentage of Ki67 positive cells in the NP/Cetux/B-Hz-DM1group (24.7 ± 3.7 %) was significantly reduced in comparison with control (41.8 ± 3.3 %) and with B-Hz-DM1-treated group (30.1 ± 2.8 %). Finally, tumor samples were stained with TUNEL to detect and quantify *in situ* the fragmented DNA, indicating irreversible cell death. The analysis revealed that, differently from what observed for tumor cell

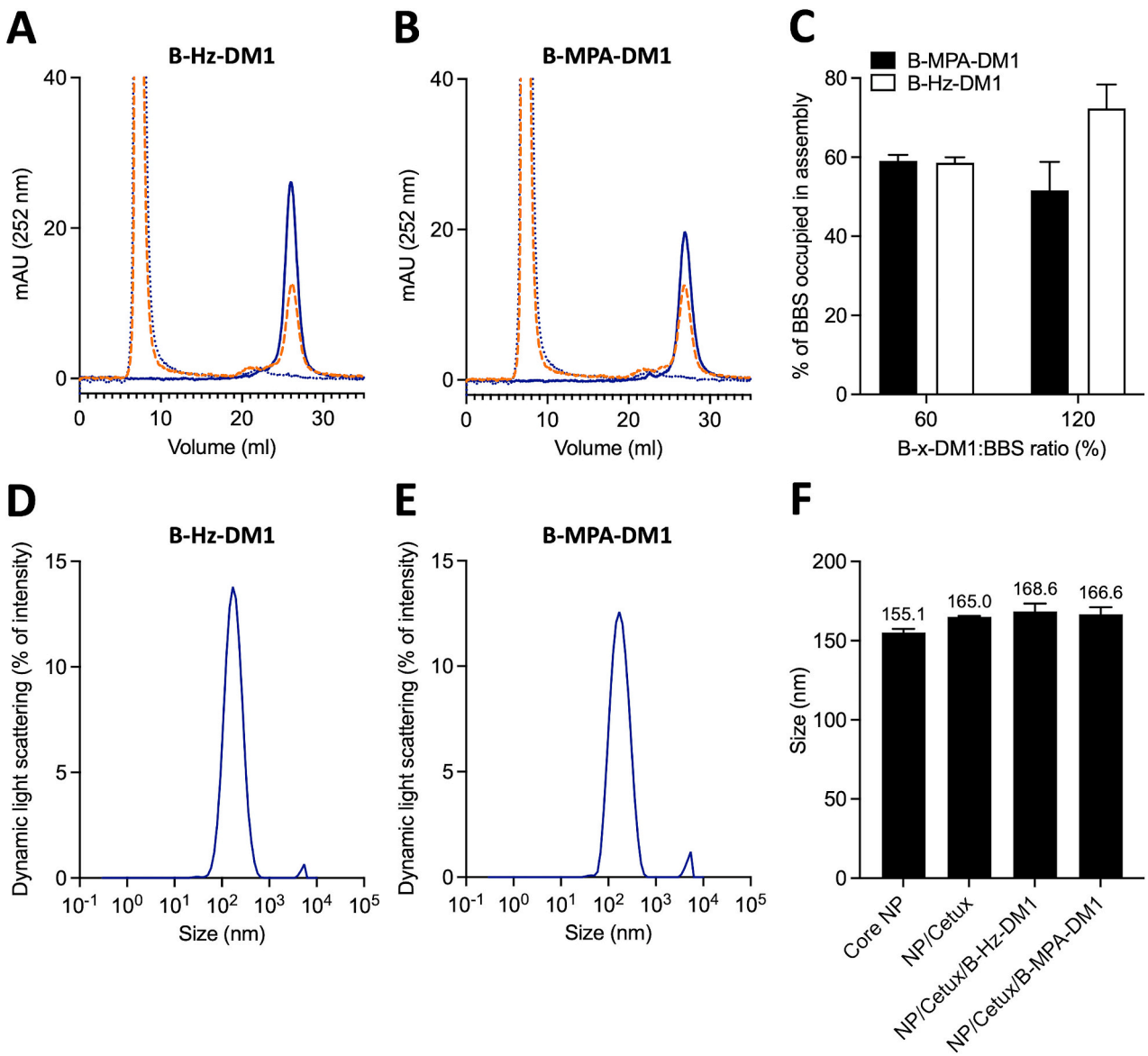

Fig. 4. Summary of pre-formulation studies. A, B) Gel permeation chromatography of B-Hz-DM1 (A) and B-MPA-DM1 (B) as free molecules (full line, blue) and when mixed with ANANAS at a biotin:BBS ratio of 60 % (dot-dot, blue) or 120 % (dash-dash, orange). The free molecules display a retention volume of 26.16 and 26.88 mL, respectively. The ANANAS NPs elute at about 8 mL. C) Loading of ANANAS with B-Hz-DM1 and B-MPA-DM1, calculated from data of panels A and B. In the x-axis, *x* indicates MPA or Hz depending on the color bar. D, E) Dynamic light scattering measurements (Intensity weighted) of ANANAS/Cetux/B-Hz-DM1 (D) and ANANAS/Cetux/B-MPA-DM1 (both at 60 % BBS coverage) (E). F) Size of Core NP, NP/Cetux, NP/Cetux/B-Hz-DM1 and NP/Cetux/B-MPA-DM1. Size of DM1 carrying formulations were measured at 60 % BBS coverage with the DM1 derivatives. Additional data can be found in the supplementary information file (Fig. S5).

proliferation, only the NP-loaded DM1 formulation (NP/Cetux/B-Hz-DM1) was able to significantly increase tumor cell death, whereas no significant effect was exerted by B-Hz-DM1 and NP/Cetux treatments (Fig. 6D).

Discussion

The main aim of this work was to evaluate the potential of a keto/hydrazone acid reversible strategy for DM1 conjugation in targeted delivery. To verify the validity of this chemical approach we exploited the ANANAS platform for conjugate evaluation.

The *in vitro* hydrolysis studies confirmed that B-Hz-DM1 has a pH-dependent stability, *i.e.* it rapidly liberates the keto derivative at acidic pH, while it is stable at neutral pH. Overall, these data suggest that at neutral pH (as in the bloodstream) the cytotoxic moiety will not be released by the NP-tethered B-Hz-DM1 complex. The release of the drug will occur only in acidic environment as in the case of hypoxic, lactic acid-rich regions of the tumor microenvironment or after target cell internalization following the endosomal-lysosomal route.

It is worth noticing that the conjugate is highly stable when positioned near the protein core of the nanoparticles, however when it is free in solution it hydrolyses relatively fast even at neutral pH (about 50 % in 24 h). It is likely that the chemical environment near the protein surface exerts a local buffering effect, which stabilizes the hydrazone bond, similar to what observed with other hydrazone drug conjugates.[4,22,23] The data collected do not allow to predict whether this buffering effect would occur also if the keto/Hz bond is used in a carrier different than ANANAS (*e.g.* in ADCs or other protein-based targeted systems). If this were not the case, it would probably be necessary to modify the spacer near to the keto moiety to improve the conjugate stability at neutral pH.

The *in vitro* cytotoxicity results obtained with the free bioconjugates demonstrated that introducing of biotin at the Maytansine C3 ester side

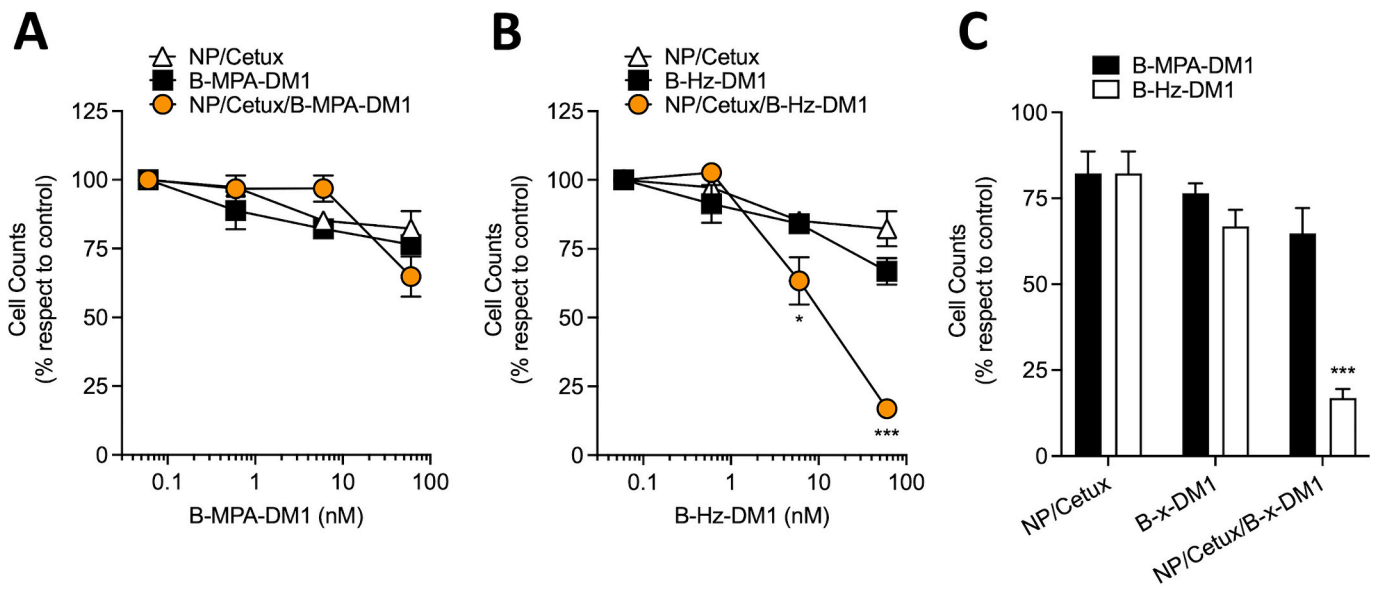

Fig. 5. Effect of NP/Cetux/DM1-derivatives on MDA-MB-231 cells. A, B) Viable cell counts of MDA-MB-231 tumor cells treated for 72 h with increasing concentration of the indicated compounds. The graphs report the percentage of live cells in respect to the control. C) Direct comparison between the effect exerted by B-MPA-DM1 (black bars) and B-Hz-DM1 (white bars) at 60 nM concentration in different loaded or unloaded formulations. On the x-axis, *x* indicates MPA or Hz depending on the color bar. The graphs report the percentage of live cells in respect to the control. For B-MPA-DM1, B-Hz-DM1, NP/Cetux/B-MPA-DM1 and NP/Cetux/B-Hz-DM1, concentration refers to effective DM1 concentration in the formulation. For NP/Cetux (unloaded), the doses are referred to the same quantity of NP/Cetux used in the NP/Cetux/B-MPA-DM1 and NP/Cetux/B-Hz-DM1 groups. Results are the mean ± SEM; $*p < 0.05$, $***p < 0.001$ *vs* unloaded (ANOVA).

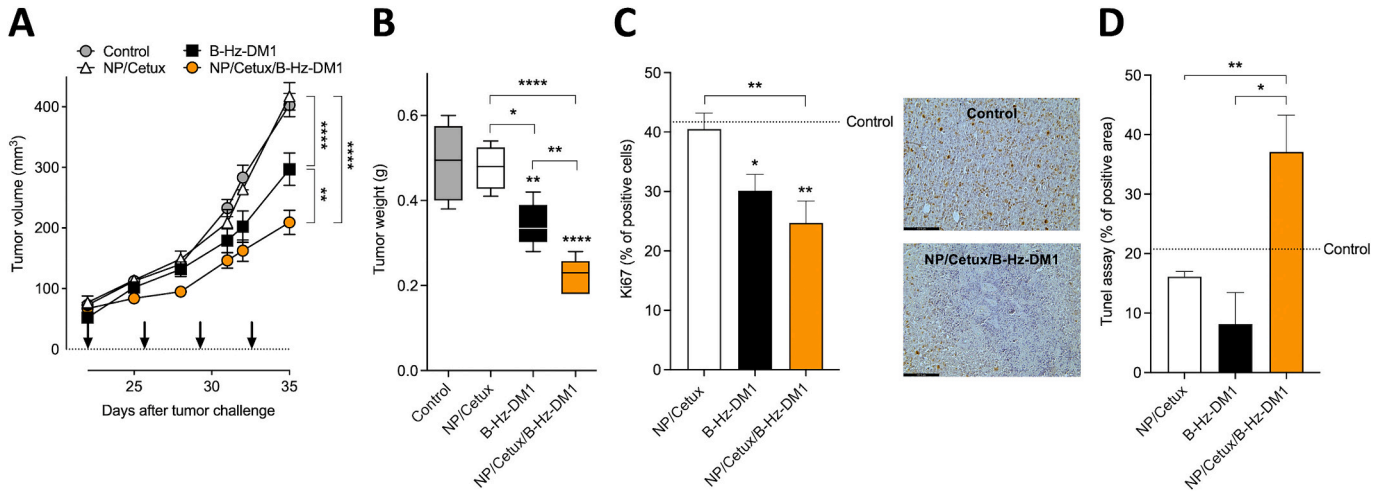

Fig. 6. Anti-tumor effect of NP/Cetux/B-Hz-DM1. Tumor growth (A) and weight (B) of MDA-MB-231 cells injected orthotopically into immune-deficient mice (n = 6/8 mice/group); arrows indicate the days of treatment. Tumors were explanted and stained for Ki67 proliferation marker (C; quantification and representative pictures) and for apoptosis (D; quantification of TUNEL staining). Results are the mean ± SEM; $*p < 0.05$, $**p < 0.01$, $****p < 0.0001$ *vs* control unless specified otherwise (ANOVA).

chain is not disruptive for DM1 activity, regardless of the type of spacer between the DM1 and biotin moieties. In fact, depending on the cell line tested, the increase in IC_{50} (and therefore the decrease in potency) compared to DM1 recorded for B-MPA-DM1 was of 7.6 to 30-fold and of 16 to 35-fold for B-Hz-DM1. These data are highly encouraging, especially when comparing the much more dramatic potency loss documented for the less hydrophobic DM1-Lys. Since the covalent and acid-reversible conjugate did not show any significant difference in these experiments, these data provide no indication as to whether the covalent or reversible strategy would be the most effective. However, potential advantage of the reversible approach stems from the data obtained with the Keto-DM1, which originates from the acid-driven hydrolysis of B-Hz-DM1. In fact, this derivative was the most active among all conjugates tested, about two-fold more potent than the covalent B-MPA-DM1 and with only 4–16-fold potency decrease compared to DM1.

Advantage of the reversible approach was further confirmed when the two biotin conjugates were compared as assembled onto the Cetux-targeted nanoparticles. In fact, when tested at 100 nM, both B-MPA and B-Hz-DM1 were more efficient when assembled onto the targeted nanoparticles; however, the reversible conjugate was about 3-fold more cytotoxic than the covalent one.

The *in vivo* validation confirmed that the hydrazone derivative B-Hz-DM1 is endowed with a relevant basal anti-tumor activity, which is in line with the release of the active keto-DM1 component. Notably, its targeted delivery by NP/Cetux/B-Hz-DM1 nanoparticles significantly increased the effect on tumor growth leading to a greater therapeutic

profile. Mechanistically, the analysis of tumor plugs revealed that the Hz/keto-DM1 reduced the cell proliferation index of cancer cells inside the tumor regardless from the fact that treatment was performed using the nano-formulation or not. Instead, a striking difference was found between these treatments in their capacity to induce apoptosis. Indeed, only the selective delivery and the preferential accumulation of keto-DM1 inside the tumor using NP/Cetux/B-Hz-DM1 was able to induce irreversible cell death as indicated by the TUNEL assay. These results indicate that a "systemic distribution" of biotin-Hz/keto-DM1 is sufficient to exert an anti-proliferative effect on cancer cells, while its accumulation in the tumor promoted by the active targeting is able to trigger cell death. Interestingly, free intracellular DM1 was proposed to lead to cell death in a concentration-dependent manner: high DM1 concentrations trigger mitotic arrest and rapid apoptotic death follow, whereas lower concentrations induce mitotic catastrophe and disrupted intracellular trafficking.[31] In any case, our findings in the tumor tissue are in line with what was observed *in vitro*, where NP/Cetux/B-Hz-DM1 displayed a stronger cytotoxic activity if compared with B-Hz-DM1.

Conclusions

Altogether the results clarify the potential of using acid-reversible keto/hydrazone chemistry for tumor-targeting of the potent DM1 moiety. This approach strongly enhances the anti-tumor potential of the cytotoxic compound while preserving a good systemic safety profile and causing a lethal accumulation at tumor site. Although these results were obtained using the cetuximab-targeted ANANAS, they are of general interest in the context of developing targeted delivery systems. The same keto/Hz-DM1 chemistry can be adopted within different targeted geometries, such as in ADCs.

As a methodological note, we would like to point out the advantage of using the ANANAS tool for conjugate comparative purposes. This tool permits the comparison of different drug derivatives while keeping other variables, known to influence the efficacy of targeted delivery systems, constant. These variables include the nature and chemical modification of the targeting agent (in this case, biotin-Cetuximab) and the ratio between the active molecule and the targeting antibody agent (DAR; Drug-to-Antibody Ratio) in ADCs. In principle, this allows for faster screening and comparison of drug conjugates from molecular design to *in vivo* validation.

Finally, the fact that B-Hz-DM1 was capable of inducing irreversible cell death *in vivo*, specifically when formulated within the cetux/NP formulation, together with the high biocompatibility and poor immunogenic profile demonstrated by this class of nanocarriers,[19,22,23,25,32] suggests that this specific assembly may be worth of further investigation towards future translation to clinical application.

Funding information

This work was funded by the University of Padova, Morpurgo PRID-DSF 2019. R.R. was supported by Associazione Italiana per la Ricerca sul Cancro (AIRC IG 2019 – ID. 23151) and is grateful for the support of the Consorzio Interuniversitario per le Biotecnologie (CIB). S.R. was supported by Fondazione Cariplo (Grant ID. 2021-1563), Fondazione Umberto Veronesi and Fondazione Camillo Golgi. I.S. and S.P. are grateful to AIRC for support (grant IG2022, no. 27271 to I.S., and fellowship no. 26584 to S.P). M.M, A.M and I.S. thank PNRR CN3 spokes 8 (M.M.) and 2 (I.S. and A.M.) for financial support.

CRediT authorship contribution statement

Elisa Schiavon: Writing – review & editing, Investigation, Formal analysis, Data curation. **Sara Rezzola:** Writing – review & editing, Investigation, Formal analysis, Data curation. **Erica Filippi:** Investigation. **Marta Turati:** Investigation. **Sofia Parrasia:** Investigation, Formal analysis. **Simone Bernardotto:** Investigation. **Martina Stocco:** Investigation. **Ildikò Szabò:** Writing – review & editing, Resources, Funding acquisition. **Andrea Mattarei:** Supervision, Resources, Funding acquisition. **Roberto Ronca:** Writing – review & editing, Writing – original draft, Supervision, Resources, Funding acquisition, Data curation, Conceptualization. **Margherita Morpurgo:** Writing – review & editing, Writing – original draft, Supervision, Resources, Funding acquisition, Data curation, Conceptualization.

Declaration of competing interest

None.

Data availability

All data generated or analyzed during this study are included in this published article and its supplementary information files.

Appendix A. Supplementary data

Detailed synthesis of B-MPA-DM1 (4), B-Hz-DM1 (12) and Keto-DM1 (13) and RP-HPLC analysis; detailed stability studies on compound 12; synthesis and characterization of biotin-PEG5kDa cetuximab; size measurements of core and functionalized nanoformulations. Supplementary data to this article can be found online at [doi:https://doi.org/10.1016/j.nano.2024.102784].

References

1. Drago JZ, Modi S, Chandarlapaty S. Unlocking the potential of antibody–drug conjugates for cancer therapy. *Nat Res*. 2021;6:327–344.
2. Zolot RS, Basu S. *Million RP. Antibody-Drug Conjugates*. 2013.
3. Mitchell MJ, Billingsley MM, Haley RM, Wechsler ME, Peppas NA, Langer R. Engineering precision nanoparticles for drug delivery. *Nat Rev Drug Discov*. 2021;20(2):101–124.
4. Roncato F, Rruga F, Porcù E, et al. Improvement and extension of anti-EGFR targeting in breast cancer therapy by integration with the Avidin-Nucleic-Acid-Nano-Assemblies. *Nat Commun*. 2018;9(1).
5. Chehelgerdi M, Chehelgerdi M, Allela OQB, et al. Progressing nanotechnology to improve targeted cancer treatment: overcoming hurdles in its clinical implementation. *BioMed Central Ltd*. 2023;22(169):1–103.
6. Chen H, Lin Z, Arnst KE, Miller DD, Li W. Tubulin inhibitor-based antibody-drug conjugates for cancer therapy. In: *MDPI AG*. 2017.
7. Goldmacher VS, Chittenden T, Chari RVJ, Kovtun YV, Lambert JM. Antibody–drug conjugates for targeted cancer therapy. *Annu Rep Med Chem*. 2012;47:349–366.
8. Jain N, Smith SW, Ghone S, Tomczuk B. *Current ADC Linker Chemistry*. New York LLC: Springer; 2015.
9. Kostova V, Désos P, Starck J-B, Kotschy A. *Pharmaceuticals The Chemistry Behind ADCs*. 2021.
10. Sun X, Widdison W, Mayo M, et al. Design of antibody-maytansinoid conjugates allows for efficient detoxification via liver metabolism. *Bioconjug Chem*. 2011;22(4):728–735.
11. Kellogg BA, Garrett L, Kovtun Y, et al. Disulfide-linked antibody-maytansinoid conjugates: optimization of in vivo activity by varying the steric hindrance at carbon atoms adjacent to the disulfide linkage. *Bioconjug Chem*. 2011;22(4):717–727.
12. Erickson HK, Widdison WC, Mayo MF, et al. Tumor delivery and in vivo processing of disulfide-linked and thioether-linked antibody-maytansinoid conjugates. *Bioconjug Chem*. 2010;21(1):84–92.
13. Junutula JR, Flagella KM, Graham RA, et al. Engineered thio-trastuzumab-DM1 conjugate with an improved therapeutic index to target human epidermal growth factor receptor 2-positive breast cancer. *Clin Cancer Res*. 2010;16(19):4769–4778.
14. Abedi M, Cohan RA, Mahboudi F, et al. Novel trastuzumab-DM1 conjugate: synthesis and bio-evaluation. *J Cell Physiol*. 2019;234(10):18206–18213.
15. Erickson HK, Lewis Phillips GD, Leipold DD, et al. The effect of different linkers on target cell catabolism and pharmacokinetics/pharmacodynamics of trastuzumab maytansinoid conjugates. *Mol Cancer Ther*. 2012;11(5):1133–1142.
16. Morpurgo M, Radu A, Bayer EA, Wilchek M. DNA condensation by high-affinity interaction with avidin. *J Mol Recognit*. 2004;17(6):558–566.
17. Pignatto M, Realdon N, Morpurgo M. Optimized avidin nucleic acid nanoassemblies by a tailored PEGylation strategy and their application as molecular amplifiers in detection. *Bioconjug Chem*. 2010;21(7):1254–1263.
18. Morpurgo M, Facchin S, Pignatto M, Silvestri D, Casarin E, Realdon N. Characterization of multifunctional nanosystems based on the avidin-nucleic acid interaction as signal enhancers in immuno-detection. *Anal Chem*. 2012;84(7):3433–3439.
19. Morpurgo M, Buda A, Facchin S, et al. Detection of a fluorescent-labeled avidin-nucleic acid nanoassembly by confocal laser endomicroscopy in the

microvasculature of chronically inflamed intestinal mucosa. *Int J Nanomedicine*. 2015;10:399.
20. Casarin E, Lucchese L, Grazioli S, et al. A new ELISA using the ANANAS technology showing high sensitivity to diagnose the bovine rhinotracheitis from individual sera to pooled milk. *PloS One*. 2016;11(1).
21. Facchin S, Digiglio L, D'Incà R, et al. Discrimination between ulcerative colitis and Crohn's disease using phage display identified peptides and virus-mimicking synthetic nanoparticles. *Nanomedicine*. 2017;13(6):2027–2036.
22. Bruna Violatto M, Casarin E, Talamini L, et al. Dexamethasone conjugation to biodegradable Avidin-Nucleic-Acid-Nano-Assemblies promotes selective liver targeting and improves therapeutic efficacy in an autoimmune hepatitis murine model article. *ACS Nano*. 2019;13(4):4410–4423.
23. Ongaro A, Violatto MB, Casarin E, et al. The mode of dexamethasone decoration influences avidin-nucleic-acid-nano-assembly organ biodistribution and in vivo drug persistence. *Nanomedicine*. 2022;40, 102497.
24. Bernardotto S, Frasson I, Faravelli S, et al. Efficient SARS-CoV-2 infection antagonization by rhACE2 ectodomain multimerized onto the Avidin Nucleic-Acid-NanoASsembly. *Biomaterials*. 2023;122394.
25. Bigini P, Previdi S, Casarin E, et al. In vivo fate of Avidin-Nucleic Acid Nanoassemblies as multifunctional diagnostic tools. *ACS Nano*. 2014;8(1):175–187.
26. Sims GEC, Snape TJ. A method for the estimation of polyethylene glycol in plasma protein fractions. *Anal Biochem*. 1980;107(1):60–63.
27. Green NM. Avidin. *Adv Protein Chem*. 1975;29(C):85–133.
28. Wilchek M, Bayer EA. *[2] Introduction to Avidin-Biotin Technology*. 1990:5–13.
29. Ran W, Liu X, Chang L, et al. Self-assembling mertansine prodrug improves tolerability and efficacy of chemotherapy against metastatic triple-negative breast cancer. *J Control Release*. 2020;318:234–245.
30. Griffin P, Hill WA, Rossi F, Boohaker R, Stinson K, Sherman I. High anti-tumor activity of a novel alpha-fetoprotein-maytansinoid conjugate targeting alpha-fetoprotein receptors in colorectal cancer xenograft model. *Cancer Cell Int*. 2023;23 (1).
31. Barok M, Joensuu H, Isola J. Trastuzumab emtansine: mechanisms of action and drug resistance. *Breast Cancer Res*. 2014;16(2):3378.
32. Violatto MB, Pasetto L, Casarin E, et al. Development of a nanoparticle-based approach for the blood–brain barrier passage in a murine model of amyotrophic lateral sclerosis. *Cells*. 2022;11(24):4003.